Gravitational Influences on Magnetic Field Structure in Accretion Disks

by

Kristiana E. Schneck

Submitted to the Department of Physics
in partial fulfillment of the requirements for the degree of

Bachelor of Science

at the

MASSACHUSETTS INSTITUTE OF TECHNOLOGY

June 2010

Author .....
Department of Physics
May 7, 2010

Certified by .....
Professor Bruno Coppi
Professor of Physics
Thesis Supervisor

Accepted by .....
Professor David E. Pritchard
Senior Thesis Coordinator, Department of Physics

Gravitational Influences on Magnetic Field Structure in Accretion Disks

by

Kristiana E. Schneck

Submitted to the Department of Physics
on May 7, 2010, in partial fulfillment of the
requirements for the degree of
Bachelor of Science

Abstract

Black holes and compact objects are often surrounded by structures known as accretion disks which consist of ionized plasma. Due to the immense forces present in the disk, interesting and complex magnetic field structures can be set up within the disk. The influence of gravity on these structures is explored via a higher-order expansion of the gravitational potential. We consider several cases: the case when the Lorentz force is negligible and the case when the Lorentz force becomes significant in the dynamics of the disk. When the Lorentz force is negligible, we find using the Ferraro Co-rotation Theorem that the strength of the magnetic field increases near the event horizon. As the strength of the Lorentz force increases and it is included in our analysis, we discover that it leads to a periodic "crystal" structure of concentric rings of current. This structure is significantly affected by gravitational forces: we find a solution to the equations of motion that shows a composite structure within the disk. We discuss the general relativistic effects near the event horizon using the Pseudo-Newtonian potential in this limit. In addition, we consider an alternate derivation of the equation of motion describing the behavior of the magnetic field and discuss its consequences.

Thesis Supervisor: Professor Bruno Coppi
Title: Professor of Physics

Acknowledgments

I would like to thank Prof. Bruno Coppi for introducing me to the fascinating world of plasma astrophysics and for his invaluable assistance in preparing this thesis. I would also like to thank Paola Rebusco for giving me a broader view of astrophysics, and Obi Ohia for his help with some of the hairier mathematics.

The community of MIT has been a wonderful place for me to learn and grow, both as a physicist and a human being. The Department of Physics has been an excellent environment where I have been challenged and taught to "think like a physicist," and this is largely due to the intelligence of the faculty and my fellow students. In addition, the opportunity to pursue a second degree in music has given me a very different perspective of academic life, and has made me a much more well-rounded person.

Last but not least, I would like to thank my friends and family for their constant support, long discussions on everything from mathematics to metaphsyics to music theory, and for laughing at my terrible physics jokes. I don't think I could have survived MIT without you.

Contents

Chapter 1

Introduction and Physical Context

1.1 Black Holes in the Universe

Black holes exhibit some of the most mysterious and fascinating phenomena in the universe. They draw the general public's attention to some of the more abstract areas of physics, but more importantly, they provide opportunities for physicists to test Einstein's theory of general relativity and other theories in modern physics.

Near the end of their lifetimes, very massive stars undergo catastrophic explosions, leaving a small massive core. This core subsequently collapses, leaving a compact object such as a neutron star or black hole. For a resulting mass between about 1.4 and 3 solar masses, this yields a compact object known as a neutron star, but for larger masses, a stellar-mass black hole is formed. Another type of black hole, known as a supermassive black hole, with mass in the range of millions to billions of solar masses, can be found in the center of many galaxies.

It is not possible to directly observe a black hole due to its gravitational effects on electromagnetic radiation, but many likely candidates have been identified by the object's effect on its surroundings. A stellar-mass black hole is often accompanied by an accretion disk, which is the source of many interesting emissions, including radio, optical, and X-ray radiation and powerful jets of matter and energy. If the black hole is accompanied by a normal star, it also possible to draw conclusions about the nature of the unseen object based on the orbital motion of the companion star.

There is a theorem that states that black holes have "no hair"–that is, they are completely characterized by three quantities: mass, charge, and angular momentum. A simple solution to Einstein's field equations exists for a non-spinning, non-charged black hole. Known as the Schwarszchild metric, this solution is given by

$$ds^2 = \left(1 - \frac{R}{R_g}\right) c^2 dt^2 - \frac{dr^2}{\left(1 - \frac{R}{R_g}\right)} - r^2 d\Omega^2 \tag{1.1}$$

where $R_g = \frac{2GM_*}{c^2}$ is the Schwarzschild radius. This solution clearly becomes singular at $R = R_g$, a location known as the event horizon.

The event horizon is the "point of no return" for material falling onto a black hole. From a classical standpoint, the event horizon is the radius at which the escape velocity exceeds the speed of light. Clearly, nothing, not even light, can escape once it has passed below this radius, making it impossible to observe a black hole in the way that one observes a normal star.

The form of the Schwarzschild metric also shows that the presence of a black hole severely warps space-time. For comparison, the metric for flat space has $g_{tt} = -1$ and $g_{rr} = 1$. Because of this severe warping, there exists an innermost stable circular orbit, or ISCO, at a radius of the order of R_g. Outside this radius, orbits are stable, allowing for the creation of accretion structures and binary systems involving a normal star or another black hole. Below this radius, an object in orbit will eventually fall into the black hole or spiral out to infinity. This is a purely relativistic phenomenon, as orbits are stable down to $R = 0$ in classical Newtonian physics.

The generalization of the Schwarzschild metric to describe a spinning black hole is known as the Kerr metric. This metric shows even more severe warping of space-time due to the angular momentum of the black hole, denoted by the parameter a_*:

$$a_* = \frac{cJ}{GM_*^2} \tag{1.2}$$

where J is the angular momentum of the black hole, and $0 \leq a_* < 1$.

The angular momentum of a Kerr black hole has an extreme effect on space-time

immediately surrounding the hole. The pull of the black hole is so strong, that in a region known as the ergosphere, space begins to rotate along with the black hole. This is known as frame-dragging, and it results in many very interesting phenomena. For instance, an object falling into a Kerr black hole with zero initial angular momentum will eventually begin to rotate with the black hole, even though its angular momentum remains zero due to conservation laws. The extreme rotation of the black hole also affects the regions of the accretion disk near the event horizon, and may help drive the powerful emission of matter and radiation in jets.

Far from the event horizon ($R \gg R_g$), the gravitational field is much weaker, and therefore, one can assume that Newtonian physics holds. In this limit, the momentum conservation equations of the plasma disk can be straightforwardly solved to obtain relevant information about the dynamics of the disk. We will make use of this assumption in the discussion of the dynamics of accretion disks.

1.1.1 The Pseudo-Newtonian Potential

A useful tool for discussing the physics of non-spinnig, non-charged (Schwarzschild) black holes without the need to solve the full field equations is known as the pseudo-Newtonian potential, first discussed by Paczynski and Wiita in 1980 [10]. This potential has the same basic form as the Newtonian potential for a point mass, but becomes singular at $R = R_g$, not the origin.

$$\Phi_{PN} = -\frac{GM_*}{R - R_g} \tag{1.3}$$

A comparison of the pseudo-Newtonian potential to the classical Newtonian potential is shown in Fig. 1-1. Note that, while the classical potential becomes singular at the origin, while the pseudo-Newtonian potential blows up as $R \rightarrow R_g$. Because of this fact, the pseudo-Newtonian potential reproduces many of the features of a full general relativistic analysis, including the event horizon and innermost stable circular orbit.

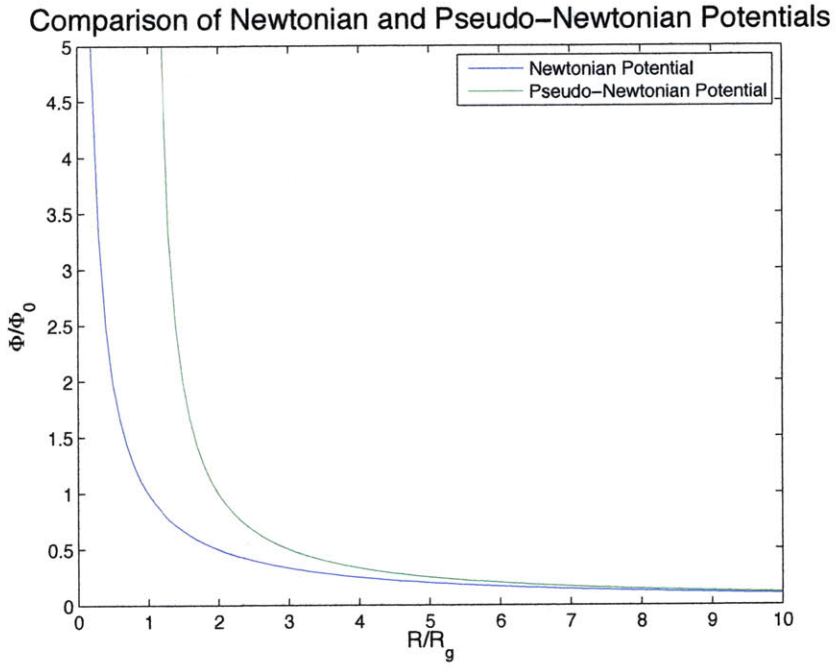

Figure 1-1: Comparison of Newtonian and pseudo-Newtonian potentials. ($\Phi_0 = -GM/R_g$)

1.2 Accretion Processes in Astrophysics

Black holes are often accompanied by normal "companion" stars, and because of their strong gravitational fields, they attract matter from these companion stars. This process forms what is known as an "accretion disk" around the black hole.

The process of accretion is the source of many interesting phenomena throughout the universe. As matter is accreted, its gravitational potential energy is converted into other forms of energy that are then radiated away. This radiation can take the form of thermal black body radiation or brehmmstrahlung radiation from collisions between electrons and ions. Bremsstrahlung radiation is discussed in more detail in Appendix A. This radiation provides an immense source of information for observational astrophysics and astronomers to study.

The dynamics of accretion were described by Shakura and Sunyaev in 1973 [12]. The Shakura-Sunyaev model requires one to solve a system of 6 equations to determine the density, pressure, temperature, and other relevant quantities of the disk. All unknown quantities are lumped into a parameter α which is associated with the

viscosity of the fluid disk.

Fig. 1-2 shows what happens when a delta-function distribution of mass around an accreting object is allowed to evolve in time. The mass spreads out, and the majority of it moves inwards. There is also a long "tail" at larger radii that serves to transport the material's angular momentum outwards.

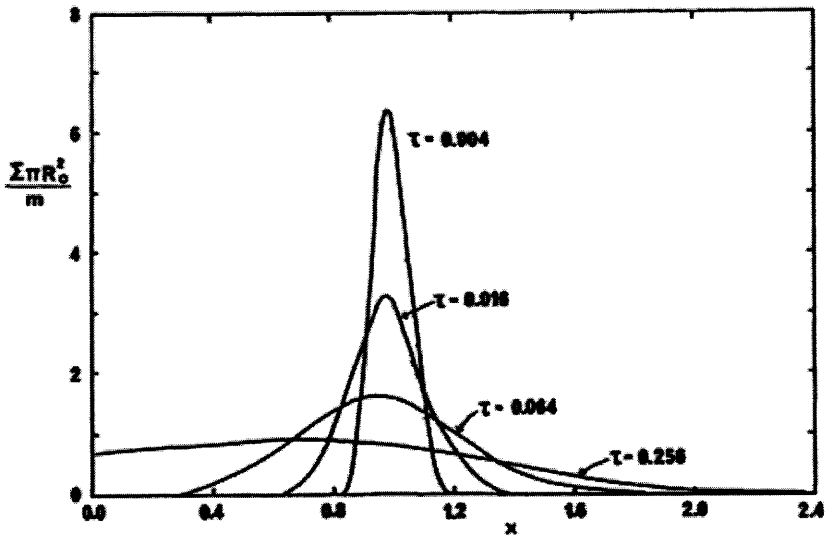

Figure 1-2: Evolution in time of a δ-function ring of mass in an accretion disk [11]. The mass spreads out and moves inwards, while angular momentum is transported outwards.

1.3 Astrophysical Plasmas

Accretion disks exist in two general types: gaseous disks, where the disk consists of ordinary matter; and plasma disks, where the accreted material is partially or fully ionized and therefore subject to electromagnetic forces. In a gaseous disk, the effects of magnetic fields are much less significant than the effects of the thermal pressure ($\beta \gg 1$), and therefore, the disk is governed by the equations of hydrodynamics. For a plasma disk, magnetic forces are much more significant, so it becomes necessary to treat the disk using the equations of magnetohydrodynamics (MHD).

1.3.1 Magnetic Field Structure in Plasmas

Plasmas generally have extremely high conductivities, and therefore can be treated as perfect conductors. Because of their nearly infinite conductivities, plasmas are subject to a constraint known as the "frozen-in law," which can be expressed as

$$\vec{E} + \frac{\Omega R}{c}\hat{e}_\phi \times \vec{B} = 0. \tag{1.4}$$

This indicates that there is no net force on the particles; the magnetic flux becomes "frozen" into the plasma.

This thesis is concerned with the behavior of the magnetic fields in a plasma disk, as determined by the magnetic surface function Ψ. The magnetic surfaces are defined by

$$\vec{B} \cdot \vec{\nabla}\Psi = 0 \tag{1.5}$$

indicating that surfaces of constant Ψ are surfaces of constant magnetic flux. The magnetic field can be derived from Ψ using the equation

$$\vec{B} = \frac{1}{R}\left(\nabla\Psi \times \hat{e}_\phi + \kappa(R,z)\hat{e}_\phi\right). \tag{1.6}$$

We assume that $\kappa = 0$ to ensure the resulting current is only in the ϕ direction. This current is given by

$$\vec{J} = \frac{c}{4\pi}\vec{\nabla} \times \vec{B} = -\frac{c}{4\pi R}\left[\frac{\partial^2\Psi}{\partial z^2} + R\frac{\partial}{\partial R}\left(\frac{1}{R}\frac{\partial\Psi}{\partial R}\right)\right]\hat{e}_\phi. \tag{1.7}$$

An interesting and useful theorem regarding the magnetic surface function was derived in 1937 by Ferraro [8]. Known as the Ferraro Corotation Theorem, it states that the frequency of rotation in a plasma disk is a function of the magnetic surfaces. That is,

$$\Omega = \Omega(\Psi). \tag{1.8}$$

Previous work ([4], [5]) has derived expressions for the magnetic surface function in the limit that the Lorentz force is stronger than the force of gravity. It was found

that, in these circumstances, Ψ exhibits a periodic "crystal" structure, as shown in Fig. 1-3. This corresponds to filaments of current which create a ring structure within the accretion disk. This ring structure has been observed in the Crab nebula pulsar system [6].

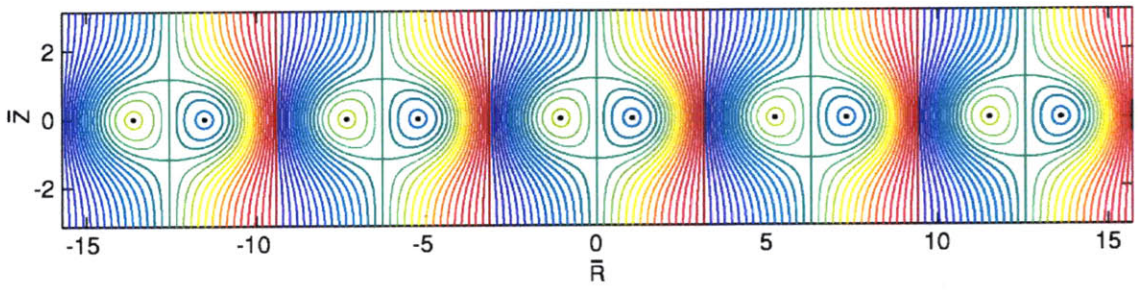

Figure 1-3: "Crystal" magnetic structure in an accretion disk [4].

In this thesis, we will use the Ferraro Corotation Theorem and the equations of motion for a plasma disk to derive an expression for the magnetic surface function Ψ when the gravitational effects of a black hole become significant.

Chapter 2

Magnetic Field Structure when the Lorentz Force is Negligible

2.1 Correction to the Rotation Frequency

To begin the discussion of the magnetic field structure in an accretion disk around a black hole, it is first necessary to derive an expression for the frequency of rotation, Ω. We assume

$$\Omega = \Omega_K + \delta\Omega \tag{2.1}$$

where $\Omega_K = \frac{GM_*}{R^3}$ is the Keplerian rotation frequency and $\delta\Omega$ is derived from the equations of motion for the disk.

In this section, the Lorentz ($J \times B$) force is assumed to be negligible compared to the forces of gravity and the pressure gradient within the plasma. In this limit, the vertical component of the momentum conservation equation is

$$-\frac{\partial p}{\partial z} - \rho\frac{GM_*}{R^3}z = 0 \tag{2.2}$$

and the radial component is

$$\rho\Omega^2 R = \frac{\partial p}{\partial R} + \rho\frac{GM_*R}{(R^2+z^2)^{3/2}}. \tag{2.3}$$

The vertical equation can be immediately solved by substituting $\rho = \frac{m_p p}{2T}$. This solution is

$$p = p_0 \exp\left[-\int_0^{z^2} \frac{dz^2}{T}\left(\frac{m_p \Omega_K^2}{4}\right)\right] \tag{2.4}$$

where p_0 is a function of R. This also defines the density ρ using the relation $\rho = \frac{m_p p}{2T}$.

$$\rho = \frac{m_p}{2T} p_0(R) \exp[-\alpha_n] \tag{2.5}$$

where $\alpha_n = \int_0^{z^2} \frac{dz^2}{T}\left(\frac{m_p \Omega_K^2}{4}\right)$

To account for the geometry of the thin disk, we expand the radial equation for $z \ll R$ and substitute $\Omega = \Omega_K + \delta\Omega$, neglecting terms higher than first order in $\delta\Omega$.

$$2\Omega_K \rho R \delta\Omega = -\rho \Omega_K^2 R \frac{3z^2}{2R^2} + \frac{\partial p}{\partial R} \tag{2.6}$$

Calculating $\frac{\partial p}{\partial R}$ from Eqn 2.4 and plugging it into Eqn 2.6 gives

$$\frac{2\delta\Omega}{\Omega_K} = -\frac{3z^2}{2R^2} + \frac{1}{R}\frac{2T}{m_p \Omega_K^2}\frac{\partial \ln p_0}{\partial R} - \frac{1}{R}\frac{2T}{m_p \Omega_K^2}\frac{\partial \alpha_n}{\partial R} \tag{2.7}$$

To calculate $\frac{\partial \alpha_n}{\partial R}$, we assume that there is no temperature gradient in the vertical direction, that is, $T = T(R)$.

$$\frac{\partial \alpha_n}{\partial R} = -\frac{m_p \Omega_K^2}{4}\frac{z^2}{T^2}\frac{\partial T}{\partial R} + \frac{m_p}{2T}\frac{z^2}{2}\frac{d\Omega_K^2}{dR} \tag{2.8}$$

Using this expression for $\frac{\partial \alpha_n}{\partial R}$ and simplifying gives the final result

$$\delta\Omega = \frac{\Omega_K}{2R^2}\left(H_0^2 \frac{\partial \ln p_0}{\partial \ln R} + \frac{z^2}{2}\frac{\partial \ln T}{\partial \ln R}\right). \tag{2.9}$$

where

$$H_0^2 = \frac{2T}{m_p \Omega_K^2}. \tag{2.10}$$

Since $z \ll R$ and H_0 is of the order of the height of the disk, it is clear that $\delta\Omega \ll \Omega_K$.

2.1.1 Alternate Temperature Profiles

In the above expression for $\delta\Omega$, we assumed that there was no temperature gradient in the z-direction. However, there exist other temperature profiles that lead to other expressions for the pressure within the disk.

The hot disk model is

$$T = T_0 \left(1 - \alpha_H \frac{z^2}{H_E^2}\right) \tag{2.11}$$

where $\alpha_H < 1$, $z^2 = H_E^2$ corresponds to the edge of the disk, and T_0 is a slow-varying function of R. Using this model, α_n becomes

$$\alpha_n = -\frac{m_p \Omega_K^2}{4T_0} \frac{H_E^2}{\alpha_H} \ln\left(1 - \frac{\alpha_H z^2}{H_E^2}\right) \tag{2.12}$$

and the pressure is

$$p = p_0 \left[1 - \frac{\alpha_H z^2}{H_E^2}\right]^{-\frac{H_E^2}{2\alpha_H H_0^2}} \tag{2.13}$$

where H_0^2 is given by Eqn 2.10.

A second alternate temperature profile is known as the cold disk model.

$$T = T_0 \left(1 + \alpha_C \frac{z^2}{H_E^2}\right) \tag{2.14}$$

In this case, the expression for α_n is

$$\alpha_n = \frac{m_p \Omega_K^2}{4T_0} \frac{H_E^2}{\alpha_C} \ln\left(1 + \frac{\alpha_C z^2}{H_E^2}\right) \tag{2.15}$$

and the pressure is

$$p = p_0 \left[1 + \frac{\alpha_C z^2}{H_E^2}\right]^{\frac{H_E^2}{2\alpha_C H_0^2}} \tag{2.16}$$

2.2 Determining the Magnetic Field Surfaces Using the Ferraro Corotation Theorem

The Ferraro Corotation theorem states that $\Omega = \Omega(\Psi)$. Inverting this, it is clear that

$$\Psi = \Psi(\Omega). \tag{2.17}$$

We will use this fact and constraints based on the physical geometry of the accreting object to derive an expression for the magnetic surfaces near the innermost stable circular orbit (ISCO).

2.2.1 Choosing the Function $\Psi(\Omega)$

Near the event horizon, we take

$$\Omega \simeq \Omega_{Kerr} + \delta\Omega \tag{2.18}$$

where Ω_{Kerr} is the rotation frequency around a Kerr (spinning, non-charged) black hole given by

$$\Omega_{Kerr} = \frac{GM_*}{R^3}\left(1 + \frac{a_*}{(8\hat{r}^3)^{1/2}}\right)^{-1} \tag{2.19}$$

where $\hat{r} = R/R_g$. Note that this expression reduces to Ω_K when $a_* = 0$.

We will choose $\Psi(\Omega)$ such that the z-component of the magnetic field vanishes at a radius R_M larger than the ISCO. This corresponds to a maximum in Ψ, resulting in magnetic surfaces that close at a radius larger than the ISCO.

$$B_z \propto \frac{\partial\Psi}{\partial R} = \frac{\partial\Psi}{\partial\Omega}\frac{\partial\Omega}{\partial R} = 0 \tag{2.20}$$

Since $\frac{\partial\Omega}{\partial R}$ is never zero for finite values of R, we must take $\frac{\partial\Psi}{\partial\Omega}$ to vanish at $R = R_M$. We choose the simple function

$$\frac{\partial\Psi}{\partial\Omega} \propto \Omega(R,z) - \Omega(R_M,z). \tag{2.21}$$

Integrating this equation yields an expression for Ψ.

$$\Psi \propto \frac{\Omega^2(R,z)}{2} - \Omega(R,z)\Omega(R_M,z) \tag{2.22}$$

2.2.2 Physical Constraints on Ψ

Now that an expression for Ψ as a function of Ω has been obtained, we will apply ad hoc constraints corresponding to the physical behavior of the system. The current must vanish for radii smaller than the ISCO, and there must also be a constraint on the z-dependent terms in Ψ that corresponds to the geometry of the thin disk.

Once these constraints are applied, the functional form of Ω becomes

$$\Omega = \sqrt{\frac{GM}{R^3}} \left\{ \left(1 + \frac{a_*}{(8\hat{r}^3)^{1/2}}\right)^{-1} - \left(\frac{z^2}{4R^2} g_T\right) F_1(R,z) \right\} \tag{2.23}$$

where we have assumed $\frac{\partial \ln p_0}{\partial \ln R}$ is negligible and defined $g_T \equiv -\frac{\partial \ln T}{\partial \ln R}$. The form of Ψ becomes

$$\Psi \propto \left[\frac{\Omega^2(R,z)}{2} - \Omega(R,z)\Omega(R_M,z) \right] F_2(R). \tag{2.24}$$

The function $F_1(R,z)$ ensures that Ψ obeys the geometry of the thin disk, and takes the form

$$F_1(R,z) = \frac{1}{1 + \left(\frac{z}{R}\right)^6}. \tag{2.25}$$

The function $F_2(R)$ is a step function that truncates the magnetic surfaces (and therefore the current) at a radius R_J near the ISCO and takes the form

$$F_2(R) = \frac{1}{2} + \frac{1}{2} \frac{(R - R_J)}{(n^2 + (R - R_J)^2)^{1/2}} \tag{2.26}$$

with $n \sim 0.1$ and R_J is of the order of R_g.

2.3 Behavior of Ψ at Small and Large Scales

Figs. 2-1 and 2-2 show the behavior of Ψ at small ($R \sim R_g$) and large ($R \gg R_g$) scales, respectively, for R in units of R_g and z in arbitrary units. These plots use the values $R_M = 2.5$, $n = 0.1$, $R_J = 1.5$, $g = 1.5$, and $a_* = 0.95$.

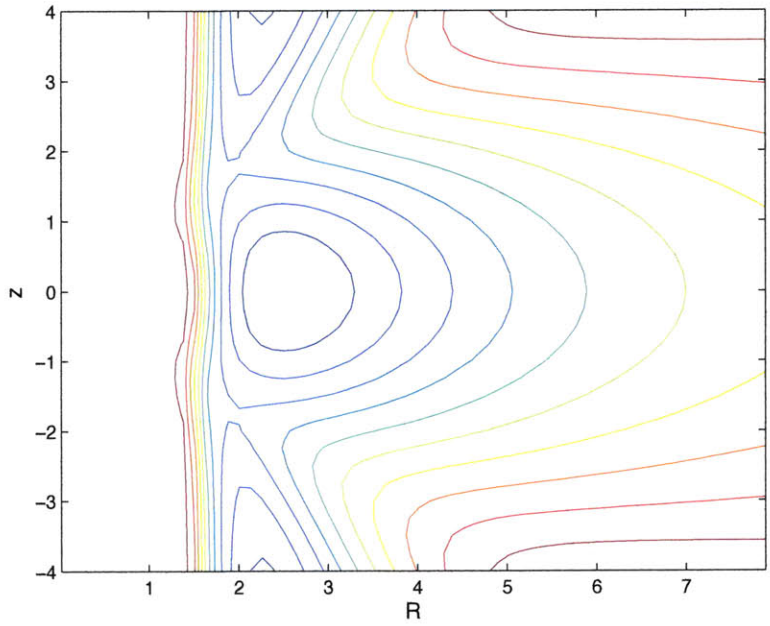

Figure 2-1: Plot of Ψ = constant (Eqn. 2.24) near the event horizon.

As per the assumptions made in choosing the functional form of Ψ, Fig. 2-1 shows that the magnetic surfaces close near the event horizon. The function goes to zero for $R < R_J$, showing that a current cannot be supported for radii smaller than the ISCO. The closed magnetic surfaces are located within the confines of the disk and create a ring of current near the event horizon.

Fig. 2-2 shows the large-scale behavior of the magnetic surfaces. Within the disk, there is interesting behavior. Near to the event horizon, the surfaces are more dense, indicating a stronger field. The surfaces also seem to "warp" near the edges of the disk, suggesting that the gravitational force of the black hole on the plasma significantly affects the magnetic field behavior.

The behavior of Ψ when $\delta\Omega$ is included is clearly different from that of the magnetic

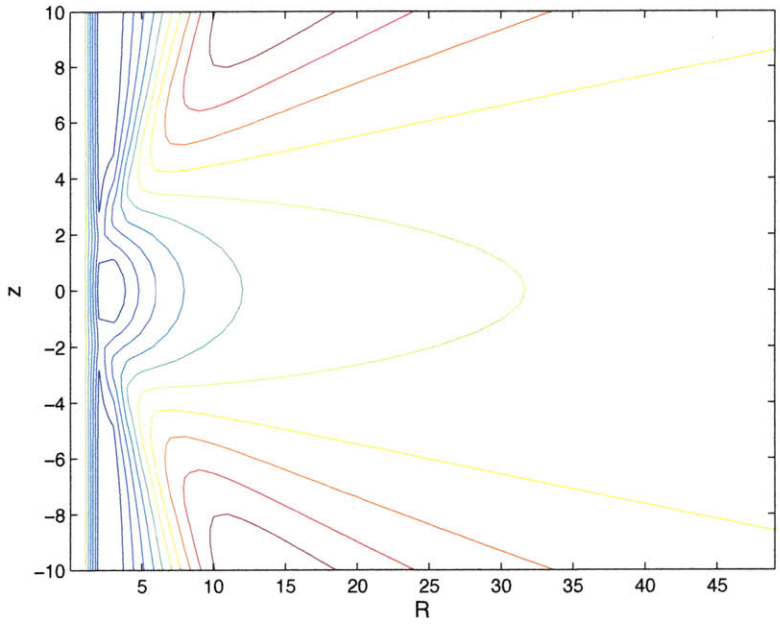

Figure 2-2: Plot of Ψ = constant at large radii.

field when no correction is taken into account. In that case, Ψ is simply a function of R, leading to magnetic surfaces that are concentric cylinders. It is clear that gravity has a warping effect on the magnetic surfaces, similar to the way gravity warps space and time.

The warping effect is shown to be especially strong near the event horizon of the black hole. This would lead to especially strong fields, which may help power the strong emissions observed in the inner regions of an accretion disk. The strong magnetic forces may also drive the ejection of matter in the form of jets.

Chapter 3

Magnetic Field Structure when the Lorentz Force Becomes Significant

3.1 Equations of Motion in this Limit

When the Lorentz force becomes significant in the dynamics of the disk, the equations of motion are

$$-\frac{\partial p}{\partial z} - \rho\frac{GM_*}{R^3}z + \frac{1}{c}(J_R B_\phi - J_\phi B_R) = 0 \tag{3.1}$$

and

$$\rho\Omega^2 R = \frac{\partial p}{\partial R} + \rho\frac{GM_* R}{(R^2+z^2)^{3/2}} - \frac{1}{c}(J_\phi B_z - J_z B_\phi). \tag{3.2}$$

In the subsequent analysis, we will assume that the current is purely in the ϕ direction.

Using the definition of the magnetic surface given in Chapter 1, the vertical component of the equation of motion (Eqn 3.1) becomes

$$-\frac{\partial p}{\partial z} - \rho\Omega_K^2 z - \frac{1}{4\pi R^2}\left[\frac{\partial^2\Psi}{\partial z^2} + \frac{\partial^2\Psi}{\partial R^2} - \frac{1}{R}\frac{\partial\Psi}{\partial R}\right]\frac{\partial\Psi}{\partial z} \simeq 0. \tag{3.3}$$

The third term in the square brackets is subsequently neglected due to the slow variation of Ψ with R, giving

$$-\frac{\partial p}{\partial z} - \rho\Omega_K^2 z - \frac{1}{4\pi R^2}\left[\frac{\partial^2\Psi}{\partial z^2} + \frac{\partial^2\Psi}{\partial R^2}\right]\frac{\partial\Psi}{\partial z} \simeq 0. \tag{3.4}$$

Following the same reasoning, the radial component (Eqn 3.2) becomes

$$2\Omega_K R\rho\delta\Omega \simeq \frac{\partial p}{\partial R} - \frac{3z^2}{2R}\rho\Omega_K^2 + \frac{1}{4\pi R^2}\left[\frac{\partial^2\Psi}{\partial z^2} + \frac{\partial^2\Psi}{\partial R^2}\right]\frac{\partial\Psi}{\partial R}. \tag{3.5}$$

This varies from previous work [4] by the term $\frac{3z^2}{2R}\rho\Omega_K^2$, which is due to the first-order expansion of the gravitational term $\rho\frac{GM_*R}{(R^2+z^2)^{3/2}}$ for $z \ll R$. This indicates that the strength of the force of gravity is comparable to the Lorentz force.

We assume that there is a strong "seed" magnetic field B_0 in the z-direction, with corresponding magnetic surfaces $\Psi_0 = \Psi_0(R)$ that are concentric cylinders. There is also an internal field associated with the current density J_ϕ. This current creates a magnetic field B_i that is represented by the magnetic surface function Ψ_1. Under these considerations, Eqns 3.4 and 3.5 become

$$-\frac{\partial p}{\partial z} - \rho\Omega_K^2 z - \frac{1}{4\pi R^2}\left[\frac{\partial^2\Psi_1}{\partial z^2} + \frac{\partial^2\Psi_1}{\partial R^2}\right]\frac{\partial\Psi_1}{\partial z} \simeq 0. \tag{3.6}$$

and

$$2\Omega_K R\rho\delta\Omega \simeq \frac{\partial p}{\partial R} - \frac{3z^2}{2R}\rho\Omega_K^2 + \frac{1}{4\pi R^2}\left[\frac{\partial^2\Psi_1}{\partial z^2} + \frac{\partial^2\Psi_1}{\partial R^2}\right]\left\{\frac{\partial\Psi_0}{\partial R} + \frac{\partial\Psi_1}{\partial R}\right\}. \tag{3.7}$$

When the $\frac{3z^2}{2R}\rho\Omega_K^2$ gravitational term is negligible, these equations have been solved in the limit that the thermal pressure is larger than the magnetic pressure ($\beta > 1$) [4] and as β approaches unity [5].

As in the previous chapter, we use the validity of the Ferraro corotation theorem to deduce useful information about the equations of motion.

$$\Omega(\Psi) = \Omega(\Psi_0 + \Psi_1) \tag{3.8}$$

Expanding this for $\Psi_0 \gg \Psi_1$ gives

$$\Omega(\Psi) = \Omega(\Psi_0) + \Psi_1\frac{d\Omega}{d\Psi_0} \tag{3.9}$$

suggesting that $\delta\Omega = \Psi_1 \frac{d\Omega}{d\Psi_0}$. We will consider the case where the force of gravity is comparable to the Lorentz force, so we add this term to that derived in Chapter 2 (Eqn. 2.9).

We expand the vertical equation (3.6) for $p \equiv \bar{p} + \hat{p}$, where $\bar{p}$ varies over a scale of order R, and $\hat{p}$ varies over a scale of order $k_0 \sim \partial/\partial R$. This also allows us to define $\rho \equiv \bar{\rho} + \hat{\rho}$. The vertical equation then becomes

$$\frac{\partial \bar{p}}{\partial z} + \Omega^2 z \bar{\rho} = 0 \tag{3.10}$$

for large scale behavior. The solution has the same form as Eqn 2.4.

The equation for behavior on a smaller scale is

$$-\frac{\partial \hat{p}}{\partial z} - \Omega^2 z \hat{\rho} - \frac{1}{4\pi R_0^2}\left[\frac{\partial^2 \Psi_1}{\partial z^2} + \frac{\partial^2 \Psi_1}{\partial R^2}\right]\frac{\partial \Psi_1}{\partial z} \simeq 0. \tag{3.11}$$

where R_0 is a reference distance from the origin. This will be solved simultaneously with the radial equation (3.7), which is written as

$$\begin{aligned} &-2\Omega R_0(\bar{\rho}+\hat{\rho})\delta\Omega - \frac{3z^2}{2R_0}(\bar{\rho}+\hat{\rho})\Omega^2 + \frac{1}{4\pi R_0^2}\left[\frac{\partial^2 \Psi_1}{\partial z^2} + \frac{\partial^2 \Psi_1}{\partial R^2}\right]\frac{\partial \Psi_0}{\partial R} \\ &\simeq -\frac{\partial}{\partial R}\left[\hat{p} + \frac{1}{8\pi R_0^2}\left(\frac{\partial \Psi_1}{\partial R}\right)^2\right] - \frac{1}{4\pi R_0^2}\left(\frac{\partial^2 \Psi_1}{\partial z^2}\right)\frac{\partial \Psi_1}{\partial R}. \end{aligned} \tag{3.12}$$

3.2 Solution to the Linearized Equations

To gain a physical understanding of the behavior of the magnetic field, we make approximations to obtain simpler, linear equations for Ψ_1. Non-linear terms in Ψ_1 and terms that vary over a scale distance much smaller than R_0 can be neglected in the limit that $\partial\Psi_1/\partial R \ll \partial\Psi_0/\partial R$, or equivalently, $B_{zi} \ll B_{z0}$. In this limit, the radial equation is

$$2\Omega R_0 \bar{\rho}\delta\Omega \simeq \frac{1}{4\pi R_0^2}\left[\frac{\partial^2 \Psi_1}{\partial z^2} + \frac{\partial^2 \Psi_1}{\partial R^2}\right]\frac{\partial \Psi_0}{\partial R} - \frac{3z^2}{2R_0}\bar{\rho}\Omega^2 \tag{3.13}$$

We define

$$\delta\Omega = \Psi_1 \frac{d\Omega}{d\Psi_0} + \delta\Omega_g \tag{3.14}$$

where

$$\delta\Omega_g = -\frac{\Omega_K}{2R^2}\left(H_0^2 g_P + \frac{z^2}{2} g_T\right) \tag{3.15}$$

is the correction to the rotational frequency due to gravitational effects derived in Chapter 2 and $g_P \equiv -\partial \ln p_0/\partial \ln R$ and $g_T \equiv -\partial \ln T/\partial \ln R$ are positive quantities to ensure that the corresponding pressure and temperature gradients are negative.

Eqn 3.13 can be simplified by noting that

$$\frac{d\Omega}{d\Psi_0} = \frac{d\Omega}{dR} \Big/ \frac{d\Psi_0}{dR} \tag{3.16}$$

and

$$k_0^2 \equiv \frac{3\Omega^2}{v_{Az0}^2} \tag{3.17}$$

where the Alfvén velocity is $v_{Az0}^2 \equiv (\partial\Psi_0/\partial R)^2/(4\pi\rho_0 R_0^2)$. Also, $2\Omega\frac{d\Omega}{dR} = -\frac{3\Omega^2}{R_0}$ for the Keplerian potential. We define $\bar{\rho} \equiv \rho_0 D(z^2)$, and therefore Eqn. 3.13 becomes

$$k_0^2 D(z^2)\Psi_1 + \left(\frac{\partial^2}{\partial R^2} + \frac{\partial^2}{\partial z^2}\right)\Psi_1 \simeq \frac{2\Omega R_0 D(z^2)}{v_{Az0}^2}\frac{d\Psi_0}{dR}\delta\Omega_g - k_0^2\frac{z^2}{2}D(z^2)B_{z0} \tag{3.18}$$

where $B_{z0} = -(\partial\Psi_0/\partial R)/R_0$.

The density profile, localized over a distance $\Delta_z < H_0$, is

$$D(z^2) = 1 - \frac{z^2}{H_n^2} \tag{3.19}$$

where $H_n^2 \sim H_0^2$.

Then we expand Eqn 3.19 to lowest order in the parameter $\epsilon_z = 1/(k_0 H_n)$, yielding

$$-k_0^2\Psi_1 \simeq \frac{\partial^2\Psi_1}{\partial R^2} \tag{3.20}$$

This has a solution of the form

$$\Psi_1(R,z) = \tilde{\Psi}_1(z)\sin(k_R[R-R_0]) \tag{3.21}$$

where $\tilde{\Psi}_1$ is an even function of z and $k_R = k_0 + \delta k_R$.

Substituting for $\delta\Omega_g$ and expanding to next order, we obtain the equation

$$-\frac{z^2}{H_n^2}\tilde{\Psi}_1 + \frac{2\delta k_R}{k_0}\tilde{\Psi}_1 + \frac{1}{k_0^2}\frac{\partial^2}{\partial z^2}\tilde{\Psi}_1 \simeq \frac{1}{\sin\bar{R}}\left[\frac{2H_0^2}{3}B_{z0}g_P - \frac{z^2}{2}B_{z0}\right] \tag{3.22}$$

where $\bar{R} = k_R[R-R_0]$.

The solution to this equation takes the form

$$\tilde{\Psi}_1(z) = \tilde{\Psi}_1^0\,(y_h + y_p) \tag{3.23}$$

where the homogeneous solution is the lowest eigensolution

$$y_h = \exp\left(-\frac{z^2}{2\Delta_z^2}\right) \tag{3.24}$$

with $\Delta_z^2 = H_n/k_0$ and the eigenvalue $\delta k_R = 1/(2H_n)$.

To find the particular solution, we first write Eqn 3.23 in dimensionless form.

$$\frac{\partial^2 y}{\partial\bar{z}^2} + \left(1-\bar{z}^2\right)y \simeq \frac{1}{\sin\bar{R}}\left[\frac{2H_0^2}{3\Delta_z^2}\tilde{B}g_P - \frac{\bar{z}^2}{2}\tilde{B}\right] \tag{3.25}$$

where $\bar{z} \equiv z/\Delta_z$ and $\tilde{B} \equiv H_n^2 B_{z0}/\tilde{\Psi}_1^0$ is the dimensionless field strength (which can be either positive or negative).

We then renormalize this equation for $\tilde{y} = y/\tilde{B}$ and define the parameter $\hat{h}^2 \equiv H_0^2/\Delta_z^2 > 1$.

$$\frac{\partial^2\tilde{y}}{\partial\bar{z}^2} + \left(1-\bar{z}^2\right)\tilde{y} \simeq \frac{1}{\sin\bar{R}}\left[\frac{2\hat{h}^2}{3}g_P - \frac{\bar{z}^2}{2}\right] \tag{3.26}$$

This equation will have a solution of the form

$$\tilde{y}(\bar{R},\bar{z}) = \frac{f(\bar{z})}{\sin\bar{R}} \tag{3.27}$$

where $f(\bar{z})$ is an even function of $\bar{z}$.

Plugging this solution into the above equation gives

$$f''(\bar{z}) + \left(1 - \bar{z}^2\right) f(\bar{z}) \simeq \frac{2\hat{h}^2}{3} g_P - \frac{\bar{z}^2}{2} \tag{3.28}$$

As before, this has the solution

$$f(\bar{z}) = \exp\left(-\frac{\bar{z}^2}{2}\right) + f_p \tag{3.29}$$

One method for finding the particular solution is discussed in the appendices. This solution does not correspond to physical behavior, so in the subsequent analysis, we ignore the effects of the particular solution.

3.2.1 Approximate Form of the Magnetic Field

If we assume that the inhomogeneous solution f_p is zero everywhere, the full expression for Ψ_1 becomes

$$\Psi_1(\bar{R}, \bar{z}) = \tilde{\Psi}_1^0 \exp\left(-\frac{\bar{z}^2}{2}\right) \sin \bar{R} + H_n^2 B_{z0} \exp\left(-\frac{\bar{z}^2}{2}\right) \tag{3.30}$$

A plot of this function for two cases, $\tilde{B} < 1$ and $\tilde{B} > 1$, is shown in Fig. 3-1.

Interesting behavior occurs in both cases ($\tilde{B} > 1$ and $\tilde{B} < 1$); however, the behavior is markedly different for the two cases. For $\tilde{B} < 1$, the structure features a series of "O" points with alternating sign at $\bar{z} = 0$, whereas for $\tilde{B} > 1$, it is a series of alternating "X" and "O" points.

We also consider the limiting cases, $\tilde{B} \to 0$ and $\tilde{B} \to \infty$. In the case of $\tilde{B} \to 0$, $\tilde{\Psi}_1^0 / H_n^2 \gg B_{z0}$, indicating that the internal magnetic field is much stronger than the external "seed" field. The first term of Eqn 3.30 dominates the field, and its structure approaches that of the "classical" structure seen below, with a series of symmetric rings with opposing signs. In the case of $\tilde{B} \to \infty$, $\tilde{\Psi}_1^0 / H_n^2 \ll B_{z0}$, and the external field dominates the dynamics of the disk. The second term of Eqn 3.30 dominates in

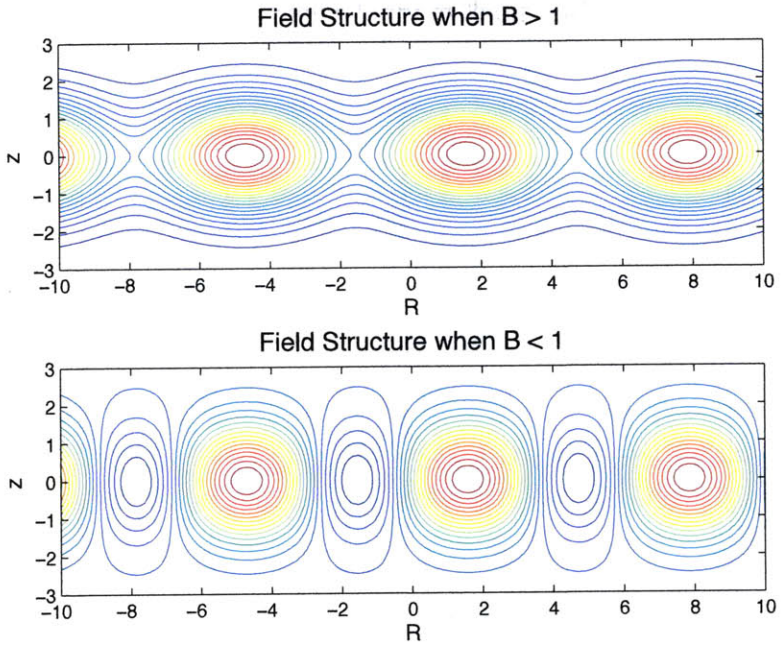

Figure 3-1: Field structure given by Eqn 3.30 for two cases, $\tilde{B} = 2$ (above) and $\tilde{B} = 1/2$ (below). (Note: this figure shows only the "internal" structure arising from the dynamics of the disk, not the external "seed" field.)

this case, effectively eliminating the periodic structures.

The analytical form of the magnetic structure including the external "seed" field is

$$\Psi = \Psi_1 + \Psi_0 = \tilde{\Psi}_1^0 \exp\left(-\frac{\bar{z}^2}{2}\right) \sin \bar{R} + H_n^2 B_{z0} \exp\left(-\frac{\bar{z}^2}{2}\right) + \epsilon_* \bar{R}. \tag{3.31}$$

where $\epsilon_* \sim 1/8$. Note that the expression for Ψ_0 yields a constant magnetic field in the vertical direction, as assumed in the derivation of the linear equations of motion.

3.2.2 Comparison to "Classical" Field Structure

Fig 3-2 shows the magnetic field structure in the case of weaker gravity, when the second-order expansion of the gravitational potential can be ignored. The simplest analytical expression for the internal structure (excluding the "seed" field) is

$$\Psi(R, z) \propto \sin \bar{R} \exp\left(-\frac{\bar{z}^2}{2}\right) \tag{3.32}$$

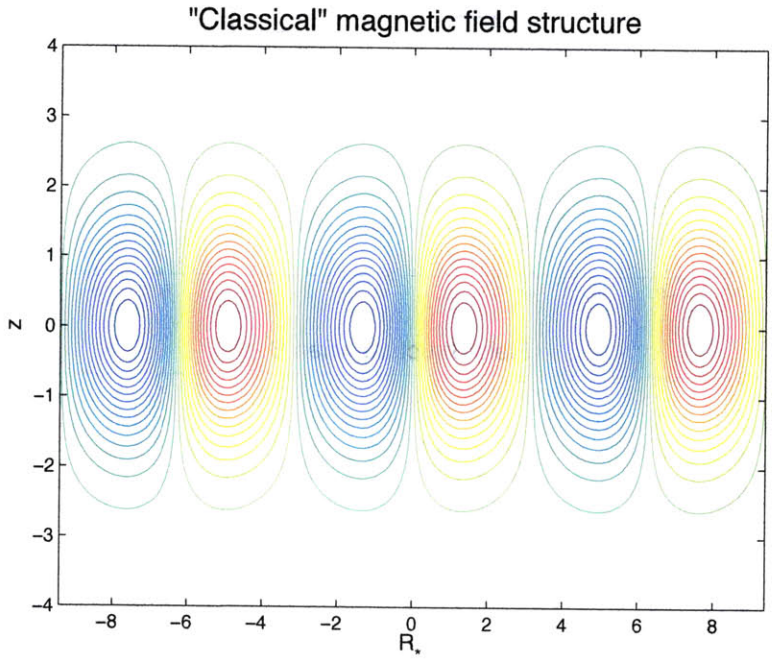

Figure 3-2: "Classical" field structure in the linear approximation when the inhomogeneous gravitational terms in Eqn 3.18 (and subsequent equations) are ignored [4].

The classical structure features a series of concentric ring structures that drive currents in opposing directions. This has been discussed in depth in Refs [4] and [5]. For this discussion, it is especially important to note the translational symmetry of the rings—the rings with negative magnitudes (blue) can be translated by $R_* = \pi$ to correspond to the rings with positive magnitudes (red and yellow).

The structure of the magnetic field for $\tilde{B} < 1$ has a similar form to the classical structure, with a series of concentric rings. However, the ring structures of the field in the case when gravitational corrections are significant does not feature the symmetry of the classical solution. The rings seen in the classical structure drive currents in the opposing directions; the structure seen in this case would suggest that one direction is favored over the other. This would imply the existence of a symmetry-breaking mechanism such as the angular momentum of the black hole; however, it is unclear whether such effects would extend to the region of the disk where these equations hold.

On the other hand, the magnetic field structure for $\tilde{B} > 1$ does not feature the

asymmetry seen in the case where $\tilde{B} < 1$. Each ring structure has the same sign and is completely identical to the neighboring rings, unlike the case for $\tilde{B} < 1$, where the a ring's neighbors are either smaller or larger. Since this corresponds to the situation where $B_{z0} > B_{zi}$, as assumed in the derivation, this situation is more likely to be the correct physical solution.

In addition to the symmetry displayed by the $\tilde{B} > 1$ case, it also shows the composite structure that has been observed in systems such as FU Orionis [7]. The region surrounding $\bar{z} = 0$ shows a highly-ordered core with structure that is similar to the "classical" case. As the magnitude of $\bar{z}$ increases, the structure enters the "envelope" regime, where the field is weaker. It is possible that the (nearly) horizontal field lines near the envelope region could power accretion onto the compact object. However, these observations also suggest that the assumption that the disk is immersed in a strong vertical magnetic field does not hold for all regions of the disk. We must therefore develop a theory where it is not necessary to assume the existence of a "seed" magnetic field. The beginnings of this theory are outlined in Chapter 4.

3.3 Linearized Equations of Motion in the Pseudo-Newtonian Potential

As in section 3.2.1, we take the approximate (linearized) configuration equation in the limit that $B_{zi} \ll B_{z0}$, this time using the pseudo-Newtonian potential. We note that this is an approximate and somewhat limited discussion, since the above analysis holds at a reference distance R_0 that is much larger than the event horizon radius R_g, while the effects of the pseudo-Newtonian potential only become significant as $R \to R_g$.

The frequency of rotation Ω in the pseudo-Newtonian potential is

$$\Omega_{PN}^2 = \frac{GM_*}{R(R - R_g)^2} \tag{3.33}$$

Taking the derivative of this gives a useful expression:

$$2\Omega\frac{d\Omega}{dR} = -\Omega_{PN}^2\left[\frac{3R-R_g}{R(R-R_g)}\right] \tag{3.34}$$

This reduces to the classical expression in the limit that $R_g \to 0$.

Noting that $\frac{d\Omega}{d\Psi_0} = \frac{d\Omega}{dR}/\frac{d\Psi_0}{dR}$ and using the expression for $d\Omega/dR$ given above, this becomes

$$\frac{\Omega_{PN}^2}{v_{Az0}^2}\left[\frac{3R-R_g}{R-R_g}\right]D(z^2)\Psi_1 + \frac{\partial^2\Psi_1}{\partial z^2} + \frac{\partial^2\Psi_1}{\partial R^2} \simeq -k_0^2\frac{z^2}{2}D(z^2)B_{z0} \tag{3.35}$$

where $D(z^2) = \bar{\rho}/\rho_0 \simeq 1-z^2/H^2$, $v_{Az0}^2 \equiv (d\Psi_0/dR)^2/(4\pi\rho_0^2R_0^2)$ and $B_{z0} = -(\partial\Psi_0/\partial R)/R_0$.

Proceeding as before, we expand this equation to lowest order in ϵ_z. This yields

$$\frac{\kappa_g}{3}\left[\frac{3\hat{r}-1}{\hat{r}-1}\right]\Psi_1 \simeq -\frac{\partial^2}{\partial\hat{r}^2}\Psi_1 \tag{3.36}$$

where $\hat{r} = R/R_g$ and $\kappa_g = k_0^2R_g^2$.

A plot of the numerical solution to this equation, with $\kappa_g = 100$ and the initial conditions $\Psi_1(R_g) = 0$ and $\Psi_1'(R_g) = 1$ is shown in Fig 3-3. This solution shows the oscillatory behavior seen in the classical solution, but the amplitude and frequency of the oscillation increase for $R \sim R_g$. This is due to the strength of the gravitational potential at that point, and is similar to the increase in the strength of the magnetic field near the event horizon seen in the case where the Lorentz force is negligible (in Ch 2). As expected, this solution becomes purely sinusoidal for $R \gg R_g$.

It is also necessary to consider the various scaling distances within this problem. The reference distance R_0 is much larger than the Schwarzchild radius R_g, and the wave vector $k_0 \sim \partial/\partial R \gg 1/R_0$. However, it is important to note that the period of the ring structure is much larger than the Schwarzchild radius ($k_0^{-1} \gg R_g$), which suggests that the case shown in Fig 3-3 ($\kappa_g = 100$), is a very extreme case. It is interesting to note that, for $\kappa_g \sim 1$, the drastic changes in period and amplitude seen in Fig 3-3 essentially disappear, leaving a nearly pure sinusoid, similar to the Newtonian case. This would suggest that the behavior of the magnetic field near the

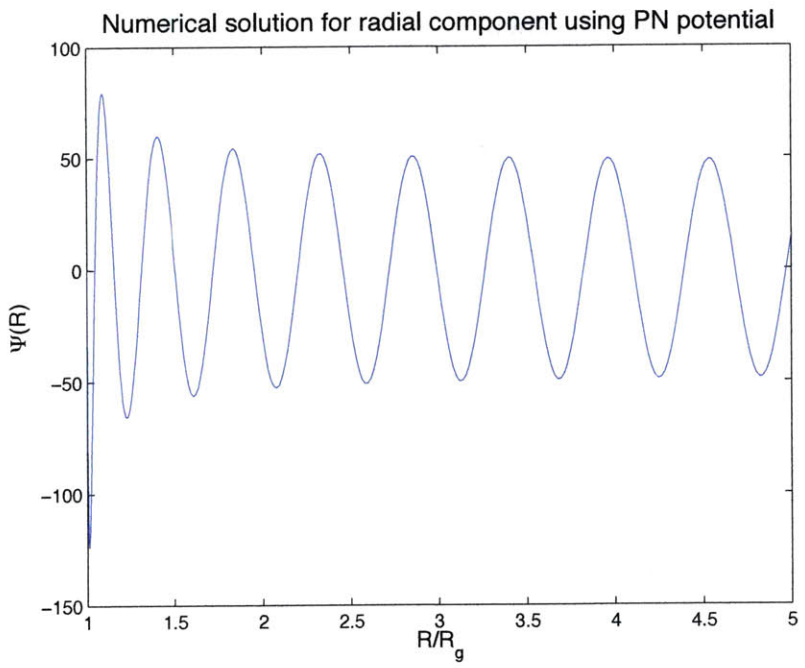

Figure 3-3: Numerical solution of 3.36, showing the behavior of Ψ near the event horizon for the extreme case of $\kappa_g = 100$.

event horizon is strongly dependent on the scale of the current rings, and therefore on the external magnetic field, as implied by the Alfvén velocity dependence of the wave vector (Eqn 3.17).

3.4 Nonlinearities in the equations of motion

To begin discussion of the nonlinear equations of motion, we define the dimensionless variable

$$Y = \frac{k_0 \Psi_1}{(\partial \Psi_0 / \partial R)} \sim \frac{B_i}{B_{z0}}. \tag{3.37}$$

The linearized approximation in the previous sections is valid for $Y \ll 1$.

The vertical equation including nonlinear terms in Ψ_1 (3.11) can be written as

$$-\frac{\partial \hat{P}}{\partial z^2} + \hat{\rho}\frac{2\pi\Omega^2}{B_{z0}^2} - \frac{\partial Y}{\partial z^2}\left[\frac{\partial^2 Y}{\partial \bar{R}^2} + \frac{1}{k_0^2}\frac{\partial^2 Y}{\partial z^2}\right] \simeq 0 \tag{3.38}$$

where we have defined $\hat{P} \equiv 4\pi\hat{p}/B_{z0}^2$.

The radial equation (3.12) is then

$$-G_\rho + k_0 R_0 \left[\frac{\partial^2 Y}{\partial \bar{R}^2} + \frac{1}{k_0^2}\frac{\partial^2 Y}{\partial z^2}\right] \simeq -k_0 \frac{\partial \hat{P}}{\partial \bar{R}} + \frac{k_0}{2}\frac{\partial}{\partial \bar{R}}\left(\frac{\partial Y}{\partial \bar{R}}\right)^2 - \frac{R_0}{k_0}\left(\frac{\partial^2 Y}{\partial z^2}\right)\frac{\partial Y}{\partial \bar{R}} \quad (3.39)$$

where the force of gravity is included in the term

$$G_\rho = \frac{4\pi}{B_{z0}^2}(\bar{\rho} + \hat{\rho})\left(2\Omega R_0 \delta\Omega + \frac{3z^2}{2R_0}\Omega^2\right) \quad (3.40)$$

The solutions to this equation when the term G_ρ can be ignored are discussed in depth in Ref [4] and are plotted in Fig 1-3. To find the solutions to next order (when G_ρ becomes significant) would require a perturbative approach, taking into account the scales on which the forces within the disk become significant.

Chapter 4

Alternate Derivation of the Equations of Motion

4.1 General Equation

As discussed in Chapter 3, it is necessary to extend our analysis to the case where it is not necessary to assume an external "seed" magnetic field. To do this, we begin with the total momentum conservation equation:

$$\nabla p + \rho\left(v \cdot \nabla v\right) + \nabla\left(\frac{B^2}{8\pi}\right) - \frac{1}{4\pi}\left(B \cdot \nabla B\right) + \rho\nabla\Phi_g = 0 \tag{4.1}$$

where

$$\Phi_g = -\frac{GM_*}{\sqrt{R^2 + z^2}} \tag{4.2}$$

We then take the curl of Eqn 4.1, and noting that $\nabla \times \nabla F = 0$, we obtain

$$\nabla \times \left[\rho\left(v \cdot \nabla v\right) - \frac{1}{4\pi}\left(B \cdot \nabla B\right)\right] + \nabla\rho \times \nabla\Phi_g = 0 \tag{4.3}$$

We then note that

$$\nabla\Phi_g = \frac{\partial\Phi_g}{\partial R}\hat{e}_R + \frac{\partial\Phi_g}{\partial z}\hat{e}_z = \frac{GM_*}{\left(R^2 + z^2\right)}\left(R\hat{e}_R + z\hat{e}_z\right) \simeq \frac{GM_*}{R^2}\left(\hat{e}_R + \frac{z}{R}\hat{e}_z\right) \tag{4.4}$$

and, assuming that $v = v_\phi(R)$,

$$v \cdot \nabla v = -\frac{v_\phi^2}{R}\hat{e}_R \tag{4.5}$$

Then, substituting 4.4 and 4.5 into 4.3 and considering only the ϕ-component, we obtain

$$\frac{\partial}{\partial z}\left[-\rho\frac{v_\phi^2}{R} - \frac{1}{4\pi}(B\cdot\nabla B)_R\right] - \frac{\partial}{\partial R}\left[-\frac{1}{4\pi}(B\cdot\nabla B)_z\right] + \frac{\partial\rho}{\partial z}\frac{GM_*}{R^2} - \frac{\partial\rho}{\partial R}\frac{GM_*}{R^3}z = 0 \tag{4.6}$$

This is the "master equation" discussed in Ref [3].

4.2 $\delta\Omega$ when the Magnetic Field is Negligible

We now take $v_\phi = R(\Omega_K + \delta\Omega)$ and neglect the magnetic field. This yields the equation

$$-\frac{\partial}{\partial z}(2\rho\Omega_K\delta\Omega R) - \frac{\partial\rho}{\partial R}\Omega_K^2 z = 0 \tag{4.7}$$

We now assume that ρ and $\delta\Omega$ are functions of both R and z, and note that $\Omega_K = \sqrt{GM_*/R^3}$. This gives

$$2R\left(\rho\frac{\partial}{\partial z}\delta\Omega + \delta\Omega\frac{\partial\rho}{\partial z}\right) + z\Omega_K\frac{\partial\rho}{\partial R} = 0 \tag{4.8}$$

If we assume that there is no temperature gradient within the plasma, the density can be taken to be

$$\rho(z,R) = \rho_0(R)\exp\left(-\frac{z^2}{2H^2}\right) \tag{4.9}$$

Plugging this into Eqn 4.8 yields

$$2R\left(\rho_0\frac{\partial}{\partial z}\delta\Omega - \delta\Omega\rho_0\frac{z}{H^2}\right) + z\Omega_K\frac{\partial\rho_0}{\partial R} = 0 \tag{4.10}$$

Dividing by $2R\rho_0$ gives

$$\frac{\partial}{\partial z}\delta\Omega - \delta\Omega\frac{z}{H^2} + \frac{z\Omega_K}{2R}\frac{\partial \ln \rho_0}{\partial R} = 0 \tag{4.11}$$

This equation takes the form

$$y' - Ayz + Bz = 0 \tag{4.12}$$

with

$$A = \frac{1}{H^2}, B = \frac{\Omega_K}{2R}\frac{\partial \ln \rho_0}{\partial R} \tag{4.13}$$

This can be solved using the method of integrating factors to obtain

$$y = y_0 \exp\left(\frac{Az^2}{2}\right) + \frac{B}{A} \tag{4.14}$$

or, substituting the values of the parameters A and B,

$$\delta\Omega\,(R,z) = \delta\Omega_0 \exp\left(\frac{z^2}{2H^2}\right) + \frac{H^2\Omega_K}{2R}\frac{\partial \ln \rho_0}{\partial R} \tag{4.15}$$

If we assume that $\delta\Omega_0 = 0$, this solution corresponds (to within a term constant in z) to that of Chapter 2 when we assume that $\rho \propto p$ and there is no temperature gradient:

$$\delta\Omega = \Omega_K \frac{H^2}{2R^2}\frac{\partial \ln \rho_0}{\partial \ln R} \tag{4.16}$$

4.3 Including the Magnetic Field

We now consider the case when the magnetic field cannot be neglected. Expanding the $(B \cdot \nabla B)$ terms gives

$$(B \cdot \nabla B)_R = \frac{1}{R}\frac{\partial \Psi}{\partial z}\left(\frac{1}{R}\frac{\partial^2 \Psi}{\partial R \partial z} - \frac{1}{R^2}\frac{\partial \Psi}{\partial z}\right) - \frac{1}{R^2}\frac{\partial \Psi}{\partial R}\frac{\partial^2 \Psi}{\partial z^2} \tag{4.17}$$

$$(B \cdot \nabla B)_z = \frac{1}{R}\frac{\partial \Psi}{\partial z}\left(\frac{1}{R^2}\frac{\partial \Psi}{\partial R} - \frac{1}{R}\frac{\partial^2 \Psi}{\partial R^2}\right) + \frac{1}{R^2}\frac{\partial \Psi}{\partial R}\frac{\partial^2 \Psi}{\partial z \partial R} \tag{4.18}$$

Plugging these expressions into Eqn 4.6 gives

$$-2R\Omega_K\frac{\partial}{\partial z}(\rho\delta\Omega)+\frac{1}{4\pi}\frac{\partial}{\partial z}\left(\frac{1}{R^3}\left[\frac{\partial\Psi}{\partial z}\right]^2-\frac{1}{R^2}\frac{\partial\Psi}{\partial z}\frac{\partial^2\Psi}{\partial R\partial z}+\frac{1}{R^2}\frac{\partial\Psi}{\partial R}\frac{\partial^2\Psi}{\partial z^2}\right)$$
$$-\quad\frac{\partial\rho}{\partial R}\Omega_K^2 z+\frac{1}{4\pi}\frac{\partial}{\partial R}\left(\frac{1}{R^2}\frac{\partial\Psi}{\partial R}\frac{\partial^2\Psi}{\partial z\partial R}+\frac{1}{R^3}\frac{\partial\Psi}{\partial R}\frac{\partial\Psi}{\partial z}-\frac{1}{R^2}\frac{\partial\Psi}{\partial z}\frac{\partial^2\Psi}{\partial R^2}\right)=0 \quad (4.19)$$

which becomes (when the derivatives are expanded)

$$-2R\Omega_K\frac{\partial}{\partial z}(\rho\delta\Omega)-\frac{\partial\rho}{\partial R}\Omega_K^2 z-\frac{1}{4\pi R^2}\frac{\partial\Psi}{\partial z}\frac{\partial^3\Psi}{\partial z^2\partial R}+\frac{1}{2\pi R^3}\frac{\partial\Psi}{\partial z}\frac{\partial^2\Psi}{\partial z^2}+\frac{1}{4\pi R^2}\frac{\partial\Psi}{\partial R}\frac{\partial^3\Psi}{\partial z^3}$$
$$-\frac{3}{4\pi R^4}\frac{\partial\Psi}{\partial z}\frac{\partial\Psi}{\partial R}+\frac{3}{4\pi R^3}\frac{\partial\Psi}{\partial z}\frac{\partial^2\Psi}{\partial R^2}-\frac{1}{4\pi R^3}\frac{\partial^2\Psi}{\partial z\partial R}\frac{\partial\Psi}{\partial R}-\frac{1}{4\pi R^2}\frac{\partial\Psi}{\partial z}\frac{\partial^3\Psi}{\partial R^3}+\frac{1}{4\pi R^2}\frac{\partial\Psi}{\partial R}\frac{\partial^3\Psi}{\partial R^2\partial z}=0 \quad (4.20)$$

We now expand for $\partial/\partial R\sim 1/\delta_R$, where $\delta_R\ll R$.

$$4\pi R^2\left[-2R\Omega_K\frac{\partial}{\partial z}(\rho\delta\Omega)-\frac{\partial\rho}{\partial R}\Omega_K^2 z\right]-\frac{\partial\Psi}{\partial z}\frac{\partial^3\Psi}{\partial z^2\partial R}+\frac{\partial\Psi}{\partial R}\frac{\partial^3\Psi}{\partial z^3}-\frac{\partial\Psi}{\partial z}\frac{\partial^3\Psi}{\partial R^3}+\frac{\partial\Psi}{\partial R}\frac{\partial^3\Psi}{\partial R^2\partial z}=0 \quad (4.21)$$

This equation has some significant differences from the equations of motion discussed in Chapter 3. First, it does not require us to assume a pressure profile to find a solution. An expression for the pressure will arise from analyzing the equation. In addition, it is not necessary to assume an external "seed" field in this case. This corresponds more closely to the composite structures discussed in Ref [3] and observationally verified in Ref [7].

Chapter 5

Discussion

5.1 Physical Consequences

5.1.1 Structure when the Lorentz Force is Negligible

In Chapter 2, we have shown that considering a higher-order expansion of the gravitational potential in the equations of motion leads to a correction to the rotation frequency that depends on the vertical coordinate z and the radial gradients of the temperature and pressure. This correction was added to the rotation frequency for a Kerr black hole and the Ferraro Co-rotation theorem was used to derive an expression for the magnetic field surfaces, Ψ. We applied appropriate physical constraints to this expression and discussed the relevant features of the resulting structures.

From this analysis, we conclude that the force of gravity have a strong influence on the structure of the magnetic field. Under classical conditions, we expect that the magnetic surfaces will be concentric cylinders; however, when the forces of gravity are included, we find that that these structures are warped within the confines of the disk. This leads to the formation of stronger fields and a ring of current near the event horizon. The strong magnetic field may help to account for some of the phenomena observed in accretion disks, including jets.

5.1.2 Effect of the Lorentz Force

When the Lorentz force is included in the dynamics of the disk, we derived the equations of motion and solved them in the linear approximation to show that a periodic "crystal" structure of current rings occurs. This behavior occurs at large radii, unlike the previous case, where only a single ring is seen near the event horizon. Like the case when the Lorentz force is negligible, the effects of the force of gravity had a significant effect on the form of the magnetic field. The periodic structure was still present, but the nature of the repeating element was altered to create new regions within the accretion disk.

We also derived the equations of motion for the Pseudo-Newtonian potential in the linear approximation, and solved the first-order equation numerically. We showed that for very small periods (high k_0 and κ_g), the period and amplitude of the magnetic field increased as we approached the event horizon. However, this was shown to be an extreme case; when $\kappa_g \sim 1$, the change in amplitude and period are much less noticeable.

5.2 Conclusions

We have shown that the forces within an accretion disk surrounding a black hole or other compact object tend to create interesting and complex magnetic field structures. When the Lorentz force can be neglected, we have derived an expression which shows that the strength of the magnetic field increases drastically near the compact object. This effect may contribute to the strong radiative emissions observed from the interior regions of accretion disks.

We have also shown that the corrections to the rotational frequency due to the higher-order expansion of the gravitational potential significantly affect the dynamics of the disk. When the Lorentz force is negiglible, the correction term $\delta\Omega$ leads to the z-dependence of the magnetic field structures. The effect of the correction terms are even more significant in the case when the Lorentz force becomes significant. In this case, the influences of strong gravity can lead to a composite structure, with a

well-ordered core surrounded by an envelope of much weaker fields.

In the case where the Lorentz force is significant, the resulting structures were derived by linearizing the equations of motion. We have derived the non-linear equations and briefly discussed the means of finding the solutions to these equations. In addition, the non-linear "master equation" (Eqn 4.6) has been derived, and its significance discussed. Future work should focus on finding the solutions to these equations and discussing their physical significance.

Appendix A

Order of magnitude estimates of several Bremsstrahlung radiation parameters

A.1 Emissivity ϵ

To get an estimate of the energy emitted by bremsstrahlung processes in a plasma, we start with Larmor formula for power radiated from an accelerating charge:

$$P = \frac{2}{3}\frac{e^2 a^2}{c^3} \tag{A.1}$$

where a is the acceleration experienced by an electron during a collision with an ion.

To calculate the acceleration, we consider Newton's second law:

$$ma = \frac{e^2}{r^2} \tag{A.2}$$

Substituting this acceleration into the power formula and ignoring factors of order unity gives:

$$P \simeq \frac{e^6}{c^3 m^2 r^4} \tag{A.3}$$

Conservation of energy gives an estimate of the velocity.

$$mv^2 \simeq \frac{e^2}{r} \tag{A.4}$$

This expression can be used to simplify Eqn. 3, yielding

$$P \simeq \frac{e^2 v^4}{c^3 r^2} \tag{A.5}$$

The energy of a photon emitted during a collision is then the power (Eqn. A.5) multiplied by the time-scale of the collision, given approximately by the classical electron radius divided by c. Setting $e^2/r \sim mc^2$ gives a formula for the energy:

$$\Delta E \simeq mc^2 \frac{v^4}{c^4} \tag{A.6}$$

An estimate of the collision rate (number of collisons per second per cm^3) can be made using simple chemical intuition:

$$\text{reaction rate} = n_e n_i \langle \sigma v \rangle \tag{A.7}$$

where σ is the scattering cross section, v is the thermal velocity and $\langle\rangle$ indicates averaging over all collisions. Setting $n_i \langle \sigma v \rangle = \nu_{ei}$, the resulting reaction rate is $n_e \nu_{ei}$, where ν_{ei} is the frequency of collisions.

The power emitted per cm^3 is then the reaction rate times the energy emitted

$$\epsilon \simeq n_e \nu_{ei} mc^2 \frac{v^4}{c^4} \tag{A.8}$$

To calculate ν_{ei}, we first determine the mean free path of an electron, $\ell = 1/n\sigma$. When combined with the velocity of the electron, this gives the frequency of collisions:

$$\nu_{ei} \sim \frac{v_{thermal}}{\ell} = n\sigma v_{thermal} \tag{A.9}$$

The cross section is calculated by estimating the impact parameter b of a bremsstrahlung

collision.

$$mv^2 \simeq \frac{Ze^2}{b} \tag{A.10}$$

Therefore

$$\sigma \simeq b^2 = \frac{Z^2e^4}{T^2} \tag{A.11}$$

Using the thermal velocity $v \simeq \sqrt{T/m}$, the expression for the frequency of collisions is approximately

$$\nu_{ei} \simeq \frac{nZ^2e^4}{\sqrt{m}T^{3/2}} \tag{A.12}$$

Substituting Eqn A.12 and the expression for the thermal velocity into Eqn A.8 gives an estimate of the energy per second per cm^3 emitted.

$$\epsilon \simeq n^2 \frac{Z^2e^4}{m^{3/2}c^2} T^{1/2} \tag{A.13}$$

This estimation is non-relativistic: the thermal velocity of the electrons is much less than the speed of light. To determine the relativistic corrections, we use the relativistic Larmor power formula

$$P \simeq \frac{e^2a^2}{c^3}\gamma^6 \tag{A.14}$$

where $\gamma = (\sqrt{1 - v^2/c^2})^{-1}$, assuming the acceleration is perpendicular to the velocity. Expanding this for $v \ll c$ gives a first-order correction that is proportional to the square of the velocity (and therefore proportional to the temperature)

$$P \simeq \frac{e^2a^2}{c^3}(1 + \alpha T) \tag{A.15}$$

where $\alpha \ll 1$.

Applying the same analysis that yielded Eqn. A.13 gives

$$\epsilon \simeq n^2 \frac{Z^2e^4}{m^{3/2}c^2} T^{1/2}(1 + \alpha T) \tag{A.16}$$

A more exact formula for the above expression was derived by Novikov and Thorne

in 1973 [9]:

$$\epsilon = \left(5.2 \times 10^{20} \frac{\text{ergs}}{\text{g s}}\right) \left(\frac{C_A f_e f_i Z^2}{A}\right) \left(\frac{\rho_0}{\text{g/cm}^3}\right) T_K^{1/2} \left(1 + 4.4 \times 10^{-10} T_K\right) \bar{\bar{G}}(T) \tag{A.17}$$

A.2 Inverse Bremsstrahlung Absorption Coefficient κ

To estimate the inverse bremsstrahlung absorption coefficient κ, we will assume that it is approximated by the wave number $k = 2\pi/\lambda$, where λ is the wavelength of the photon. This is in accordance with the definition of κ: $\kappa \propto \Im(k)$, where $\Im$ represents the imaginary part.

Inverse bremsstrahlung radiation occurs when a photon is absorbed during a collision between an ion and an electron in a plasma. We therefore expect the energy of the photon to be approximately equal to the work done on the electron during the collision.

$$\hbar c k \simeq m_e a r \tag{A.18}$$

We calculate the acceleration experienced by the electron using Newton's second law:

$$ma \simeq \frac{e^2}{r^2} \tag{A.19}$$

and therefore

$$\hbar c k \simeq \frac{e^2}{r} \simeq m(\Delta v)^2 \tag{A.20}$$

where the second equality is due to the conservation of energy.

To find Δv, we use the conservation of momentum, treating the photon as a

particle with momentum proportional to its wave number k.

$$\hbar k = \frac{\hbar\omega}{c} \simeq m\Delta v \tag{A.21}$$

Therefore,

$$\hbar ck \simeq m\left(\frac{\hbar\omega}{mc}\right)^2 \tag{A.22}$$

The absorption coefficient must be proportional to the "reaction rate" of electron-ion collisions. By dimensional analysis, we must also multiply the LHS of the above equation by the appropriate dimensionful quantities.

$$\frac{\hbar ck}{(\text{time}) \times (\text{volume})} \simeq n\nu_{ei}\frac{\hbar^2\omega^2}{mc^2} \tag{A.23}$$

The appropriate time scale for a photon is $1/\omega$, and the volume scale is approximately $\lambda^3 = (c/\omega)^3$. Plugging these into the above and solving for $k \simeq \kappa$ gives

$$\kappa \simeq n\nu_{ei}\frac{\hbar}{m\omega^2} \simeq \frac{n^2e^4\hbar}{m^{3/2}T^{3/2}\omega^2} \tag{A.24}$$

A.3 Optical Depth τ

The optical depth is related to the length parameter a, which is a measure of the radius of a plasma sphere when the flux from black-body radiation at the surface is equal to the flux of bremsstrahlung radiation [1].

The energy flux for a black body is given by the Stefan-Boltzmann law.

$$F = \sigma T^4 \tag{A.25}$$

This will be equated with the flux due to bremsstrahlung emission, which is given by the emissivity multiplied by the parameter a.

$$\sigma T^4 \simeq \frac{n^2Z^2e^4}{m^{3/2}c^2}T^{1/2}a \tag{A.26}$$

Solving for a gives

$$a \simeq \frac{\sigma m^{3/2} c^2}{n^2 Z^2 e^4} T^{7/2} \tag{A.27}$$

The optical depth τ is given by the path length L divided by the parameter a.

$$\tau \propto n^2 Z^2 L T^{-7/2} \tag{A.28}$$

As τ increases, the emission approaches that of a black body.

Appendix B

Method for finding an analytical solution to Eqn 3.28

We wish to find a particular solution to the equation

$$f''(\bar{z}) + \left(1 - \bar{z}^2\right) f(\bar{z}) \simeq H^2 - \frac{\bar{z}^2}{2} \tag{B.1}$$

where $H^2 = \frac{2\hat{h}^2}{3} g_P$.

We consider a solution of the form

$$f_p(\bar{z}) = \alpha(\bar{z})\, y_n \tag{B.2}$$

where y_n is the n^{th} eigensolution of the homogeneous equation. (In Eqn B.1, $n = 1$.) Plugging this into Eqn B.1 and multiplying by y_n gives

$$(y_n^2 \alpha')' = \left[H^2 - \frac{\bar{z}^2}{2}\right] y_n. \tag{B.3}$$

where prime denotes derivative with respect to $\bar{z}$.

Integrating this equation yields

$$y_n^2 \alpha' = \int^{\bar{z}} \left[H^2 - \frac{x^2}{2}\right] y_n(x)\, dx + C \equiv G(\bar{z}) \tag{B.4}$$

where x is a dummy integration variable and C is a constant of integration. Taking the lowest eigensolution ($y_1 = \exp(-x^2/2)$), this expression becomes

$$G(\bar{z}) = \frac{\sqrt{2\pi}}{4}\left(2H^2 - 1\right)\mathrm{erf}\left(\frac{\bar{z}}{\sqrt{2}}\right) + \frac{\bar{z}}{2}\exp\left(-\frac{\bar{z}^2}{2}\right) + C \tag{B.5}$$

where erf denotes the error function,

$$\mathrm{erf}(x) = \frac{2}{\sqrt{\pi}}\int_0^x \exp(-t^2)\,dt \tag{B.6}$$

Dividing by the lowest eigensolution $y_1^2 = \exp(-\bar{z}^2)$ and taking $C = 0$ gives

$$\alpha' = \frac{\sqrt{2\pi}}{4}\left(2H^2 - 1\right)\mathrm{erf}\left(\frac{\bar{z}}{\sqrt{2}}\right)\exp\left(\bar{z}^2\right) + \frac{\bar{z}}{2}\exp\left(\frac{\bar{z}^2}{2}\right) \tag{B.7}$$

Therefore,

$$\begin{aligned}\alpha(\bar{z}) &= \int^{\bar{z}} \frac{G(\tilde{x})}{y_n^2(\tilde{x})}\,d\tilde{x} \\ &= \frac{\sqrt{2\pi}}{4}\left(2H^2 - 1\right)\int^{\bar{z}} \exp(\tilde{x}^2)\mathrm{erf}\left(\frac{\tilde{x}}{\sqrt{2}}\right)\,d\tilde{x} + \frac{1}{2}\exp\left(\frac{\bar{z}^2}{2}\right)\end{aligned} \tag{B.8}$$

and the inhomogeneous solution becomes

$$\begin{aligned}f_p(\bar{z}) &= \exp\left(-\frac{\bar{z}^2}{2}\right)\times\left\{\frac{\sqrt{2\pi}}{4}\left(2H^2 - 1\right)\int^{\bar{z}} \exp(\tilde{x}^2)\mathrm{erf}\left(\frac{\tilde{x}}{\sqrt{2}}\right)\,d\tilde{x} + \frac{1}{2}\exp\left(\frac{\bar{z}^2}{2}\right)\right\} \\ &= \frac{\sqrt{2\pi}}{4}\left(2H^2 - 1\right)\exp\left(-\frac{\bar{z}^2}{2}\right)\int^{\bar{z}} \exp(\tilde{x}^2)\mathrm{erf}\left(\frac{\tilde{x}}{\sqrt{2}}\right)\,d\tilde{x} + \frac{1}{2}\end{aligned} \tag{B.9}$$

This solution goes very quickly to infinity as $\bar{z}$ increases, making it non-physical. If we take $2H^2 = 1$, the runaway term disappears; however, in this case, we are left with $f_p =$ constant, which does not affect the overall magnetic field structure.

Bibliography

[1] G. Bekefi, *Radiation Processes in Plasmas* (John Wiley and Sons, Inc. 1966)

[2] H. Bradt, *Astrophysics Processes* (Cambridge University Press, 2008).

[3] B. Coppi, MIT LNS Report 2010/01 (to be published in American Institute of Physics 2010).

[4] B. Coppi, *Physics of Plasmas* **12**, 057302 (2005).

[5] B. Coppi and F. Rousseau, *Astrophysical Journal*, 641: 458-470 (2006).

[6] Chandra X-ray Observatory Center NASA/CSX/SAO. ACIA/HETG Image (2002).

[7] J. F. Donati, F. Paletou, J. Bouvier, and J. Ferreira, *Nature* **438**, 466 (2005).

[8] V. C. A. Ferraro, *Monthly Notices of the Royal Astronomical Society* Vol. 97, p. 458, (1937).

[9] I. D. Novikov, and K. S. Thorne, in *Black Holes*, ed C. De Witt, B. S. De Witt. (New York: Gordon & Breach, 1973).

[10] B. Paczynski and P. J. Wiita, *Astron. Astrophys.* **88**: 23 (1980)

[11] J. E. Pringle, *Annu. Rev. Astron. Astrophys.* **19**, 137 (1981).

[12] N. I. Shakura, and R. A. Sunyaev *Astron. Astrophys*, 24:337, (1973).

[13] Shoji Kato, Jun Fukue, and Shin Mineshige. *Black-hole Accretion Disks* (Kyoto University Press, 1998)